Chemical Engineering Journal 160 (2010) 788–793

Contents lists available at ScienceDirect

Chemical Engineering Journal

journal homepage: www.elsevier.com/locate/cej

Equiaxed zinc oxide nanoparticle synthesis

Kathy Lu*, Jingzhong Zhao

Department of Materials Science and Engineering, Virginia Polytechnic Institute and State University, Blacksburg, VA 24061, USA

ARTICLE INFO

Article history:
Received 1 January 2010
Received in revised form 16 March 2010
Accepted 29 March 2010

Keywords:
Zinc oxide
Nanoparticle
Particle size
Crystalline phase
Light absorption

ABSTRACT

ZnO is widely used in many important areas, such as solar cells, piezoelectric transducers, light emitting diodes, gas sensors, and catalysts. This study is focused on equiaxed ZnO nanoparticle synthesis from aqueous solutions. The shape, size, and phase of the synthesized ZnO particles are investigated by transmission electron microscopy and X-ray diffraction. A synthesis mechanism is proposed. ZnO particle size effect on light absorption is evaluated by UV–vis spectrophotometry. The study offers a simple, better-defined, and more versatile approach for synthesis of equiaxed ZnO nanoparticles.

1. Introduction

ZnO has been extensively studied over the past years. They are widely used in many important areas, such as solar cells [1], electronics [2], light emitting diodes [3], gas sensors [4], and catalysts [5]. UV–vis absorption spectra show that absorption intensity and absorbed light wavelength increase with reaction time and ZnO particle size [6–8]. However, most of the studies are focused on the synthesis of ZnO nanorods and nano-belts because of their preferential *z* direction growth tendency [9–12]. ZnO nanoparticles of equiaxed shapes and defined crystallinity have not been readily obtained. From a different perspective, equiaxed ZnO nanoparticles can be more easily assembled into unique structures, made into thin films or bulk structures, and tailored in dimensions for novel electronic and optical properties in solar cells, transparent electronics, and light emitting diodes. This requires better understanding of ZnO nanoparticle synthesis in order to control their shape and size. Otherwise, ZnO nanorods instead of nanoparticles can easily form [13].

Many methods have been used to synthesize ZnO nanoparticles. Solid-state methods include chemical vapor deposition [14], atomic layer deposition [15], thermal decomposition [16], spray pyrolysis [17], and laser heating [18]. Liquid methods include direct precipitation [19], sol–gel method [6], and hydrolysis [20]. Among these methods, the solid-state processes produce highly aggregated particles. In contrast, the liquid-based routes have the advantage of offering well dispersed particles at low temperatures.

The sol–gel route initially proposed emphasizes boiling of an ethanolic solution of zinc acetate dihydrate to form zinc precursor [21]. Following this approach, 3.0 nm sized ZnO nanoparticles from zinc acetate derived precursor are obtained [22]. Through the reaction of zinc acetate solutions with LiOH, ZnO particles of 2–7 nm size range are obtained [6]. In recent years, many simpler methods have been pursued in order to obtain well-dispersed ZnO nanoparticles. But achieving equiaxed nanoparticle size with well defined crystallinity has been a challenge. For example, oleic acid-capped ZnO nanoparticles are obtained by the reaction between the –OH group on the ZnO nanoparticles and the –COOH group of the oleic acid [19]. Hydrothermal synthesis has been used to obtain highly crystalline ZnO nanoparticles at 120 °C [23]. ZnO particles are also obtained by precipitation from $Zn_5(CO_3)_2(OH)_6$ in an aqueous solution from room temperature to 70 °C [24]. Another recent effort in ZnO nanoparticle synthesis is using aqueous solution of zinc nitrate and tris(hydroxymethyl)aminomethane at near neutral pH and 37 °C. The as-obtained nanoparticles have 20 nm size [25]. Hexamethylenetetramine (HMT) has been used to prepare ZnO particles [26–28]. pH value, HMT, and zinc nitrate concentrations are each varied to control the particle size and shape. However, the process has not been exploited for ZnO nanoparticle synthesis. In addition, the roles of HMT in ZnO nanoparticle synthesis and the crystallinity of the ZnO particles obtained merit further investigation [29].

In this study, hexagonal wurtzite ZnO nanoparticles have been synthesized by mixing aqueous solutions of zinc nitrate and HMT. Equiaxed particles are obtained by aging the nanoparticle precursor at 300 °C. The resultant ZnO nanoparticle shape, size, and crystallinity are investigated by transmission electron microscopy

* Corresponding author at: 213 Holden Hall, Mail Code 0237, Blacksburg, USA. Tel.: +1 540 231 3225; fax: +1 540 231 8919.
E-mail address: klu@vt.edu (K. Lu).

1385-8947/$ – see front matter © 2010 Elsevier B.V. All rights reserved.
doi:10.1016/j.cej.2010.03.073

(TEM), dynamic light scattering (DLS), and X-ray diffraction (XRD). ZnO particle size effect on light absorption has been evaluated by UV–vis spectrophotometry.

2. Experimental procedures

The starting materials for the ZnO nanoparticle synthesis were zinc nitrate hydrate ($Zn(NO_3)_2{\cdot}xH_2O$) (99% purity, Alfa Aesar, Ward Hill, MA) and HMT ($C_6H_{12}N_4$) (99% purity, Alfa Aesar, Ward Hill, MA). $Zn(NO_3)_2{\cdot}xH_2O$ was dissolved in water to form 0.1 M solution. HMT was dissolved in water to form 0.5 to 2.0 M solutions. Before mixing, both kinds of solutions were stirred with magnetic stir rods at 900 rpm for 30 min at room temperature. Then the $Zn(NO_3)_2$ solution was poured into the HMT solution after the stirring rods were removed. The mixture was kept in an oven at 60 °C for 45 min with no stirring. The precipitate was filtered out through a Millipore filter (0.22 μm GV, Durapore Membrane Filters, Billerica, MA) by a vacuum pump. The filtered precipitate was dried in the oven at 60 °C. After that, it was heated to 300 °C for 1 h at 3 °C/min heating and cooling rates.

The ZnO particles obtained were dispersed in water by ultrasound. The suspension was either placed on TEM grids for particle size and shape analyses (Philips EM 420, Philips Electron Optics, Eindhoven, The Netherlands) or examined by DLS for particle size analysis (Zetasizer Nano ZS, Malvern Instruments, Inc., Southborough, MA). Also, electron diffraction was carried out for the ZnO particle phase analysis using the TEM. To further investigate the crystalline phase of the synthesized ZnO particles, high resolution X-ray diffraction (XRD) studies were carried out in an X'Pert PRO diffractometer (PANalytical B.V., EA Almelo, The Netherlands). The scan time per step was 3000 s with CuK_α radiation ($\lambda = 1.5406$ Å). The XRD voltage was 45 kV and the beam current was 40 mA. The weight change of the Zn^{2+}-containing precipitates at high temperatures was investigated by thermogravimetric analysis (STA449C/3/G Jupiter, Netzsch Instruments, Inc., Burlington, MA).

The absorption spectra were taken for the dilute suspensions of the synthesized ZnO particles (~0.125 wt%, pH ~7.0 ± 0.35) using UV–vis spectrophotometry (Evolution 300, Thermo Scientific, England) with a xenon lamp as the light source. The spectra were collected in the 200–500 nm wavelength range at 0.2 nm step size.

3. Results and discussion

3.1. HMT:$Zn(NO_3)_2$ ratio effect

During ZnO formation, the chemical process proceeds with the decomposition of the precipitating agent HMT [30]:

$$C_6H_{12}N_4 + 6H_2O \rightarrow 6H_2CO + 4NH_3 \quad (1)$$

Ammonia dissociates further to form ammonium cations and hydroxyl anions:

$$NH_3 + H_2O \rightarrow NH_4^+ + OH^- \quad (2)$$

Two processes exist for the Zn^{2+}-containing precipitate formation, depending on the solution condition:

$$Zn^{2+} + 2OH^- \Leftrightarrow Zn(OH)_2 \quad (3)$$

$$Zn^{2+} + H_2O \Leftrightarrow ZnO + 2H^+ \quad (4)$$

When the solution pH is high (alkaline solution), Eq. (3) proceeds. When the solution pH is low (acidic condition), Eq. (4) is favored based on the thermodynamic data [31]. For the specific Zn^{2+}-containing precipitate formation, there are two important aspects to consider. One is the availability of the precipitating species, such as Zn^{2+} and OH^-. The other is the function of the large molecules from the precipitating agent HMT. During Zn^{2+}-containing precipitate nucleation and growth, the solid phase that is most stable will generally precipitate first. If the pH and the Zn^{2+} concentration are both high, then $Zn(OH)_2$ formation is preferred. If the Zn^{2+} concentration is low, then $Zn(OH)_2$ formation may be suppressed and the formation of ZnO may be preferred, especially when the HMT molecules attach to the newly formed nanoparticle surfaces and prevent the accessibility of the OH^- groups to the surfaces. In this study, all the reaction solutions have a similar neutral pH value of 6.8–7.0, higher than the pH range reported for ZnO particle synthesis but also lower than the pH range reported for $Zn(OH)_2$ particle synthesis [26]. As a result, the effect of HMT is the dominant factor to consider.

Fig. 1 shows the Zn^{2+}-containing precipitate morphology and phase results when HMT:$Zn(NO_3)_2$ ratio changes from 1:1 to 20:1. The specific phases are identified by Selected Area Electron Diffraction (SAED). First, a selected area of the ZnO particles is focused and a selected area aperture is placed. The effect is to block the entire electron beam except for the small fraction passing through the aperture. Only this region contributes to the diffraction pattern. When the HMT:$Zn(NO_3)_2$ ratio is 1:1, the electron diffraction pattern is in a halo ring format and cannot be indexed (Fig. 1b). This means amorphous Zn^{2+}-containing species forms, mostly in thin, flaky $Zn(OH)_2$ format (Fig. 1a). When the HMT:$Zn(NO_3)_2$ ratio is 5:1 and higher, ZnO particles form. There are fewer particles in the view and the diffraction patterns are bright spots aligned along the rings. The rings can be indexed for phase identification (Fig. 1c–h).

A striking feature to notice is the high HMT concentration needed in order to form ZnO particles of defined crystallinity. It is often stated that HMT acts as a source of hydroxide to drive the precipitation reaction. However, it has also been argued that the HMT's role is that of a buffer. The rate of hydrolysis decreases with increasing pH. At 1:1 HMT:$Zn(NO_3)_2$ ratio, $Zn(OH)_2$ precipitate forms because of the less screening effect from the large HMT molecules. However, the amount of $Zn(OH)_2$ formed is very low because the solution is near neutral state. The precipitate has thin, flaky morphology (Fig. 1a). As the HMT:$Zn(NO_3)_2$ ratio increases to 5:1, several factors start to affect the amount of the OH^- groups. The total amount of the OH^- groups should increase because of a high amount of HMT. But the hydrolysis of HMT is also suppressed for the OH^- group release. In addition, the OH^- group availability to the ZnO particles decreases because of the screening effect from the HMT. The composition of the solution is such that ZnO is thermodynamically stable. The precipitation mechanism changes from nucleation and growth via a flaky hydroxide intermediate to formation of platy ZnO directly [32]. Flaky $Zn(OH)_2$ and platy ZnO species co-exist when the HMT:$Zn(NO_3)_2$ ratio is 5:1 (Fig. 1c) and much defined diffraction pattern starts to emerge (Fig. 1d). As the HMT:$Zn(NO_3)_2$ ratio increases to 10:1, platy ZnO species is dominant with a small amount of flaky ZnO species (Fig. 1e). The electron diffraction pattern is well defined. As the HMT:$Zn(NO_3)_2$ ratio increases to 20:1, almost all the ZnO species are plate-like (Fig. 1g) and the diffraction pattern is also well-defined (Fig. 1h). More interestingly, the particle shapes also become more elongated as the HMT:$Zn(NO_3)_2$ ratio increases (Fig. 1c, e, and g). This means there is a restructuring of $Zn(OH)_2$ amorphous structure into ZnO crystal structure when a higher content of HMT is present. Also, HMT encourages *z* direction growth into elongated ZnO shapes. These results clearly illustrate the influence of the HMT screening effect on the nucleation and growth of the ZnO particles.

When the HMT:$Zn(NO_3)_2$ ratio is 1:1, the size of the $Zn(OH)_2$ precipitate is less than 100 nm but the structure is amorphous. When the HMT:$Zn(NO_3)_2$ ratio is 5:1 or higher, the size of the precipitate is greater than 100 nm even though ZnO particles are obtained. In order to obtain ZnO nanoparticles with defined crystallinity, the process needs to be re-examined. The XRD results

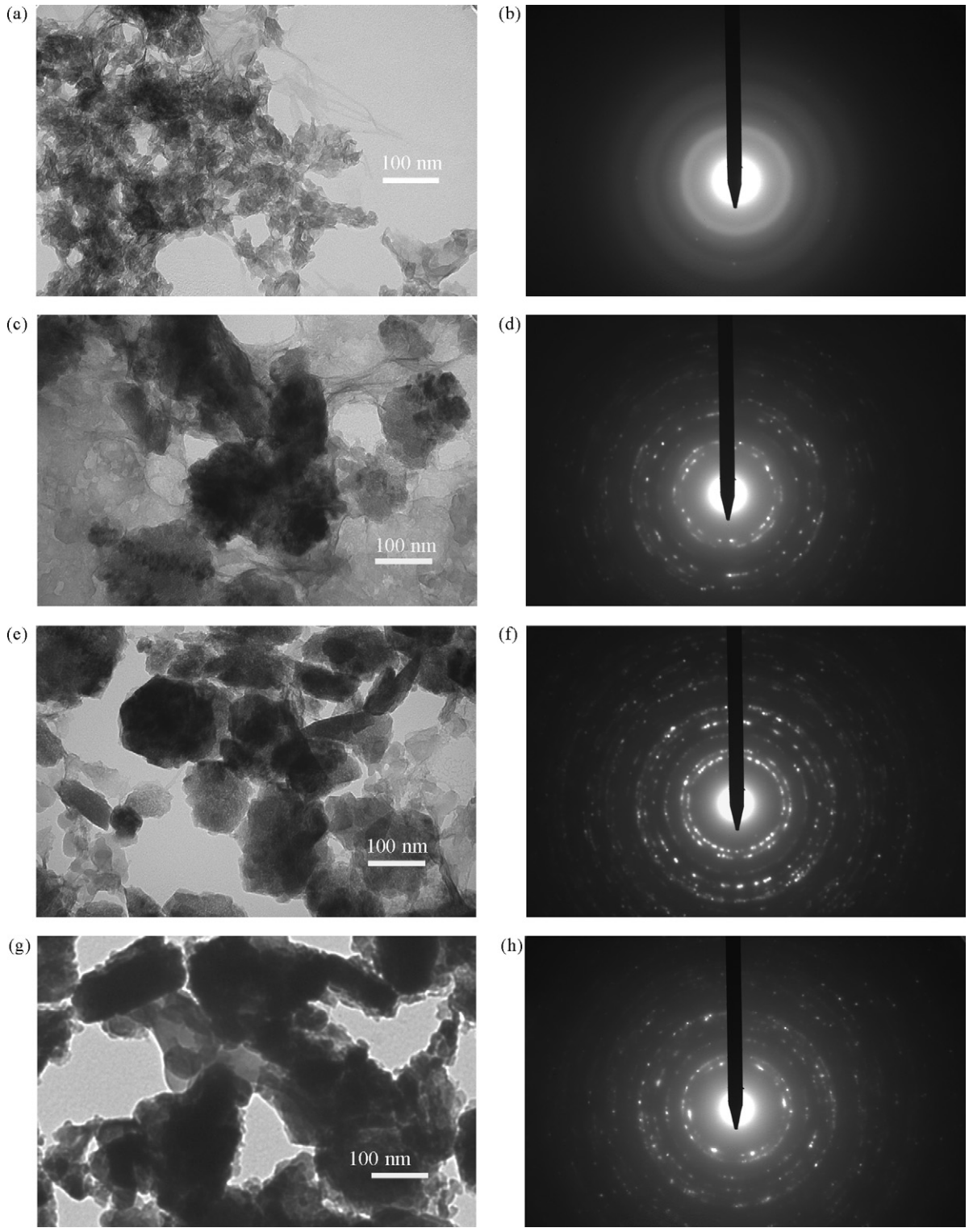

Fig. 1. $Zn(OH)_2$ to ZnO precipitate morphology and electron diffraction pattern transitions when HMT:$Zn(NO_3)_2$ ratio changes from 1:1 to 20:1. (a and b) 1:1; (c and d) 5:1; (e and f) 10:1; (g and h) 20:1.

(Fig. 2) show a consistent trend with the TEM electron diffraction patterns. At 1:1 HMT:$Zn(NO_3)_2$ ratio, the XRD peaks are poorly developed. There are two small, weak peaks at 33° and 59° but no crystalline phase can be identified. At 5:1–20:1 HMT:$Zn(NO_3)_2$ ratios, the XRD patterns show the characteristic triple peaks of ZnO at 32°, 34°, and 36°. All the peaks are well defined. The crystalline phase is identified as hexagonal ZnO (wurtzite structure JCPDS 01-076-0704).

3.2. High temperature aging effect

For most of the nanoparticle synthesis, aging at room or elevated temperature can be used for further particle size, shape, or phase refinement. In this study, the synthesized Zn^{2+}-containing precipitates have been heated to 300 °C for 1 h. Fig. 3a and b shows that the flaky $Zn(OH)_2$ precipitate in Fig. 1a and b has transformed into uniform and well-defined, hexagonal ZnO nanoparticles. By

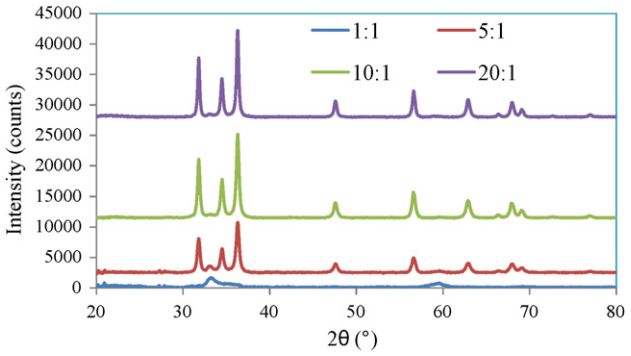

Fig. 2. XRD patterns when HMT:$Zn(NO_3)_2$ ratio changes from 1:1 to 20:1.

measuring the particle sizes from the TEM image and calculating the particle size and deviation, the result is 5.5 ± 0.99 nm. Based on the DLS measurement, the particle size is 1.4 nm (Fig. 4). The difference is believed to be a result of these different measurement techniques. The electron diffraction pattern shows well defined rings (Fig. 3b). Because the ZnO particle size is small, there are enough particles in the view and the bright spot from each particle connect and form well defined diffraction rings. At 5:1 and 10:1 HMT:$Zn(NO_3)_2$ ratios, the ZnO particles show much larger sizes. Some elongated particles appear for both 5:1 and 10:1 HMT:$Zn(NO_3)_2$ ratios. The crystalline phase remains as hexagonal wurtzite at 5:1 and 10:1 HMT:$Zn(NO_3)_2$ ratios. Because of the large particle sizes, there are fewer particles in the view; the diffracted bright spots are discrete along the diffraction rings. Fig. 3 demonstrates that high temperature aging has the effect of crystallizing the amorphous Zn-containing precipitate while refining the precipitate size.

The XRD patterns for the ZnO particles synthesized at HMT:$Zn(NO_3)_2$ ratios from 1:1 to 10:1 after high temperature aging is shown in Fig. 5. The higher than 10:1 HMT:$Zn(NO_3)_2$ ratio conditions provide hexagonal ZnO crystalline structures without high temperature aging and is not shown here. Fig. 5 indicates that the $Zn(OH)_2$ precipitate at 1:1 HMT:$Zn(NO_3)_2$ ratio condition has transformed into hexagonal ZnO crystalline structure, similar to the higher HMT:$Zn(NO_3)_2$ ratio conditions. In addition, the ZnO particle size (assuming each particle consists of one crystallite) can be estimated using Scherrer's equation:

$$\tau = \frac{K\lambda}{\beta \cos\theta} \tag{5}$$

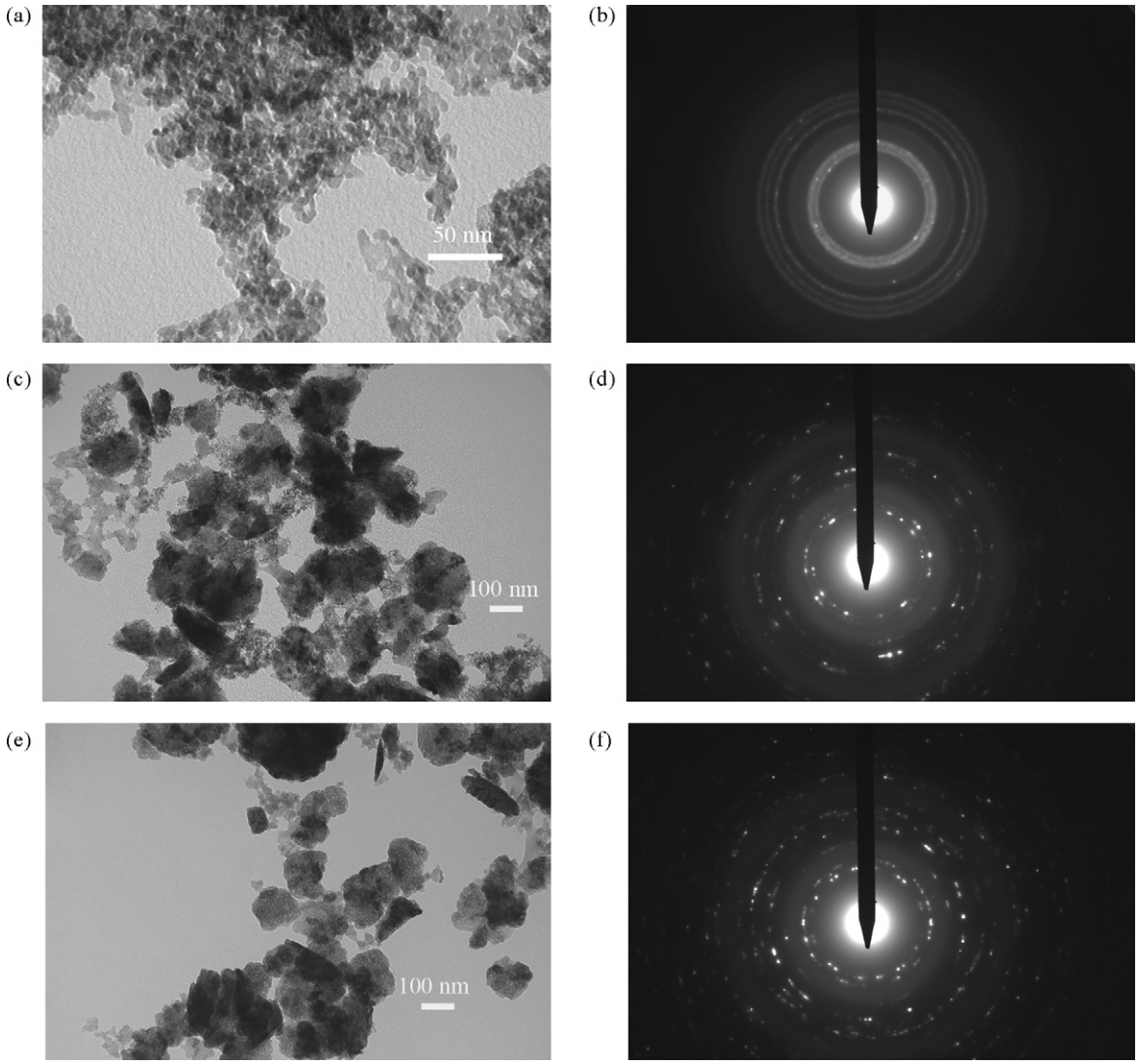

Fig. 3. TEM images and electron diffraction patterns of ZnO particles at 1:1 to 10:1 HMT:$Zn(NO_3)_2$ ratios after high temperature aging: (a and b) 1:1; (c and d) 5:1; (e and f) 10:1.

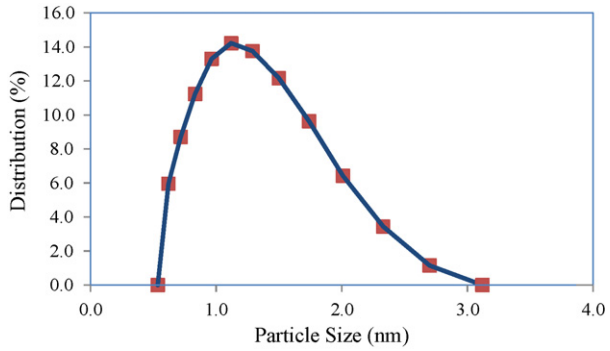

Fig. 4. ZnO particle size at 1:1 HMT:$Zn(NO_3)_2$ ratio measured by DLS.

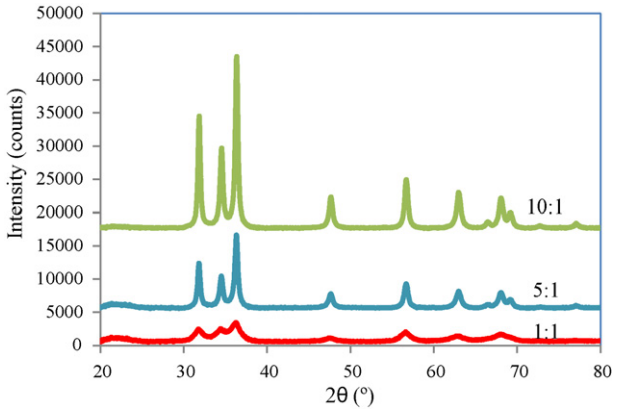

Fig. 5. XRD patterns after high temperature aging when HMT:$Zn(NO_3)_2$ ratio changes from 1:1 to 10:1.

where K is the shape factor, taken as 0.9 in this study; λ is the X-ray wavelength, 1.5406 Å in this study; β is the line broadening at half the maximum intensity in radians; and θ is the Bragg angle; τ is the mean size of the crystallite size. The ZnO particle size is calculated to be 3.0 nm. Taking into consideration of the assumptions used in the calculation, this particle size is in reasonable agreement with the measurements from the DLS and the TEM imaging. Combining Figs. 3a and b and 4, and the particle size result from Eq. (5), it means that uniform, ~3.3 nm size (taking the average from these three measurement techniques), and hexagonal ZnO particles can be synthesized using the approach discussed in this study.

3.3. Zn-containing precipitate nucleation and growth mechanism

Even though it has been suggested that HMT may act as a condensation agent, forming water and ZnO from zinc hydroxide [30], the exact process is not explained. Formation of specific precipitate species and the rate of precipitate growth are governed by the concentration of the precursors and the solution conditions. Higher concentrations of precursors are conducive for precipitate formation. The formation mechanism of the different morphology Zn^{2+}-containing precipitate can be understood as follows (Fig. 6). At low HMT:Zn^{2+} ratios, HMT adsorption onto the new precipitate is low. OH^- groups can be incorporated into the Zn^{2+}-containing precipitate. $Zn(OH)_2$ is most likely to form. Since the supply of OH^- groups from HMT is low, the chemical reaction happens at a slow rate, the precipitate amount is low, the precipitated phase is thin, and the crystalline phase is not developed. At high HMT:$Zn(NO_3)_2$ ratios, HMT acts as the precipitation barrier by blocking the availability of the OH^- groups to the precipitate surface. Also, HMT is likely to preferentially adsorb onto the high surface energy direction [0 1 1 0]. It prevents the [0 1 1 0] surface of the ZnO particles from excessive growth. ZnO can only grow in the lowest surface energy direction with a higher amount of OH^- group supply than the 1:1 HMT:$Zn(NO_3)_2$ ratio case. As a result, ZnO particles grow into thick hexagonal structures. The precipitate changes from flaky morphology to platy morphology, or even to elongated morphology. Depending on the HMT:$Zn(NO_3)_2$ ratio, flaky or platy precipitate can form along with different levels of crystallinity. The understanding of the HMT adsorption on the Zn^{2+}-containing precipitates has been partially supported by the weight change of different Zn^{2+}-containing precipitates (as synthesized) during the thermogravimetric analysis. In order to eliminate the hydroxyl group effect, the weight change above 150 °C shows that for the HMT:$Zn(NO_3)_2$ 5:1 ratio, the weight loss is 1.67 wt% more than that for the HMT:$Zn(NO_3)_2$ 1:1 ratio sample. During the high temperature aging, the Zn-containing precipitates restructure into more energy favorable shapes. For the thin flaky precipitate at 1:1 HMT:$Zn(NO_3)_2$ ratio, the precipitate spheroidizes to minimize the total surface energy. For the 5:1 and higher HMT:$Zn(NO_3)_2$ ratios, the particle size becomes smaller than the original but is still larger than that of the 1:1 HMT:$Zn(NO_3)_2$ ratio case.

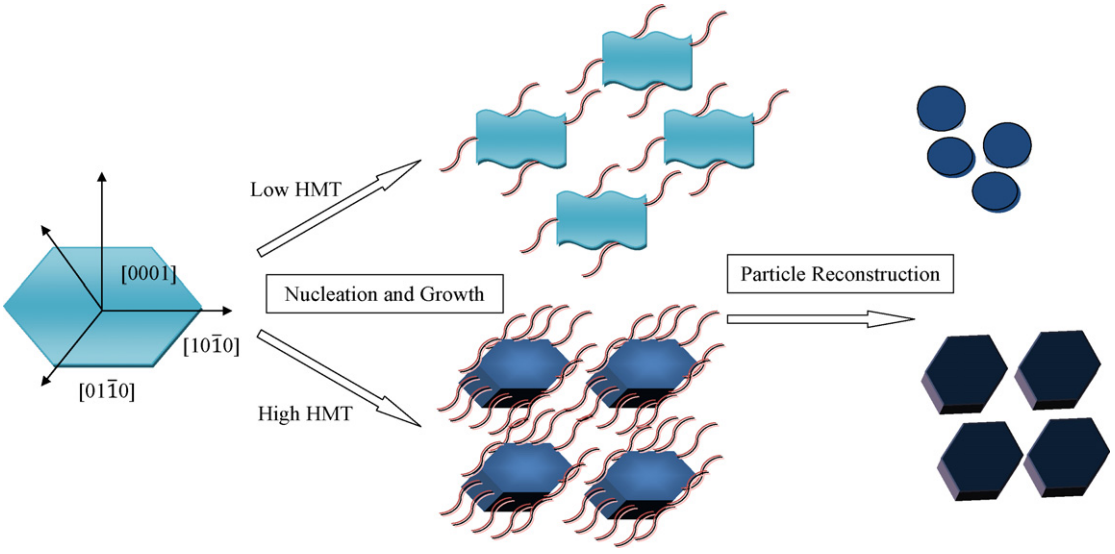

Fig. 6. ZnO-containing species nucleation and growth mechanism.

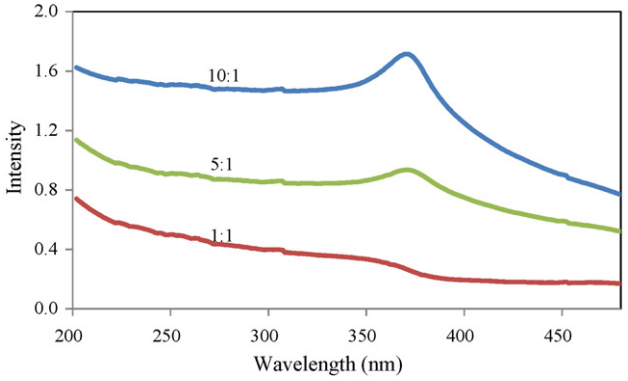

Fig. 7. ZnO particle size effect on light absorption.

In practice, this means the precipitation process has to be carefully controlled. To obtain equiaxed ZnO nanoparticles, the HMT:$Zn(NO_3)_2$ ratio should be low in order to prevent excessive ZnO preferential growth. After the precipitation of the solid phase, a high temperature process should be carried out for the precipitate to fully crystallize. If the interest is to obtain elongated, needle-shaped particles, the HMT:$Zn(NO_3)_2$ ratio should be high; additional crystallization process is not necessary [30]. However, nanosize particles are very difficult to obtain.

3.4. ZnO particle size effect on light absorption

ZnO particle size effect on light absorption is shown in Fig. 7. The absorption peak for the larger particle sizes (5:1 and 10:1 HMT:$Zn(NO_3)_2$ ratio conditions) can be easily seen at 367 nm. As the ZnO particle size decreases to ~3.3 nm, the absorption peak shifts slightly to the smaller wavelength number (360 nm) and can hardly be observed. These can be understood from twofolds. For the slight light absorption peak shift to the left, the main factor is the particle size decrease from >100 nm to ~3.3 nm. For the weak absorption peak, it is likely due to the very low concentration of the ZnO particles used (0.125 wt%) or the interference from the environment [33].

4. Conclusions

This study is focused on equiaxed ZnO nanoparticle synthesis from aqueous solutions. ZnO synthesis mechanism, phase evolution, and light absorption property are evaluated. To form equiaxed ZnO nanoparticles, the HMT:$Zn(NO_3)_2$ ratio should be low and an elevated temperature aging process is needed for crystallization. Otherwise, platy ZnO particles form and the crystalline phase is hexagonal. UV–vis absorption analysis shows that the light absorption peak shifts slightly to the smaller wavelength number as the ZnO particle size decreases to ~3.3 nm. The results offer a simple, better-defined, and more versatile procedure for the synthesis of equiaxed ZnO nanoparticles.

Acknowledgment

The authors acknowledge the financial support from National Science Foundation under grant No. CMMI-0824741.

References

[1] A. Tiwari, M. Snure, Synthesis and characterization of ZnO nano-plant-like electrodes, J. Nanosci. Nanotechnol. 8 (2008) 3981–3987.
[2] S.H. Ko, I. Park, H. Pan, N. Misra, M.S. Rogers, C.P. Grigoropoulos, A.P. Pisano, ZnO nanowire network transistor fabrication on a polymer substrate by low-temperature, all-inorganic nanoparticle solution process, Appl. Phys. Lett. 92 (2008) 154102.
[3] B. Karthikeyan, C.S.S. Sandeep, T. Pandiyarajan, P. Venkatesan, P. Philip, Optical and nonlinear absorption properties of Na doped ZnO nanoparticle dispersions, Appl. Phys. Lett. 95 (2009) 023118.
[4] J.H. Jun, J. Yun, K. Cho, I.S. Hwang, J.H. Lee, S. Kim, Necked ZnO nanoparticle-based NO_2 sensors with high and fast response, Sens. Actuators B 140 (2009) 412–417.
[5] X.F. Ma, M.R. Zachariah, Oxidation anisotropy and size-dependent reaction kinetics of zinc nanocrystals, J. Phys. Chem. C 113 (2009) 14644–14650.
[6] E.A. Meulenkamp, Synthesis and growth of ZnO nanoparticles, J. Phys. Chem. B 102 (1998) 5566–5572.
[7] G. Oskam, F.D.P. Poot, Synthesis of ZnO and TiO_2 nanoparticles, J. Sol–Gel Sci. Technol. 37 (2006) 157–160.
[8] N. Sakamoto, S. Ishizuka, N. Wakiya, H. Suzuki, Shape controlled ZnO nanoparticle prepared by microwave irradiation method, J. Ceram. Soc. Jpn. 117 (2009) 961–963.
[9] O. Akhavan, M. Mehrabian, K. Mirabbaszadeh, R. Azimirad, Hydrothermal synthesis of ZnO nanorod arrays for photocatalytic inactivation of bacteria, J. Phys. D 42 (2009) 225305.
[10] Z.Z. Zhou, Y.L. Deng, Kinetics study of ZnO nanorod growth in solution, J. Phys. Chem. C 113 (2009) 19853–19858.
[11] Y.L. Liu, Y.C. Liu, J.Y. Zhang, Y.M. Lu, D.Z. Shen, X.W. Fan, ZnO hexagonal prisms grown onto p-Si (1 1 1) substrate from poly(vinylpyrrolidone) assisted electrochemical assembly, J. Cryst. Growth 290 (2006) 405–409.
[12] S.S. Yue, J.J. Lu, J.Y. Zhang, Controlled growth of well-aligned hierarchical ZnO arrays by a wet chemical method, Mater. Lett. 63 (2009) 2149–2152.
[13] R. Chander, A.K. Raychaudhuri, Growth of aligned arrays of ZnO nanorods by low temperature solution method on Si surface, J. Mater. Sci. 41 (2006) 3623–3630.
[14] N. Reuge, R. Bacsa, P. Serp, B. Caussat, Chemical vapor synthesis of zinc oxide nanoparticles: experimental and preliminary modeling studies, J. Phys. Chem. 113 (2009) 19845–19852.
[15] T.Y. Shvareva, S.V. Ushakov, A. Navrotsky, J.A. Libera, J.W. Elam, Thermochemistry of nanoparticles on a substrate: zinc oxide on amorphous silica, J. Mater. Res. 23 (2008) 1907–1915.
[16] P. Jajarmi, Fabrication of pure ZnO nanoparticles by polymerization method, Mater. Lett. 63 (2009) 2646–2648.
[17] T. Ogi, D. Hidayat, F. Iskandar, A. Purwanto, K. Okuyama, Direct synthesis of highly crystalline transparent conducting oxide nanoparticles by low pressure spray pryolysis, Adv. Powder Technol. 20 (2009) 203–209.
[18] C. Fauteux, R. Smirani, J. Pegna, M.A. El Khakani, D. Therriault, Fast synthesis of ZnO nanostructures by laser-induced chemical liquid deposition, Appl. Surf. Sci. 255 (2009) 5359–5362.
[19] R.Y. Hong, T.T. Pan, J.Z. Qian, H.Z. Li, Synthesis and surface modification of ZnO nanoparticles, Chem. Eng. J. 119 (2–3) (2006) 71–81.
[20] G. Rodriguez-Gattorno, P. Santiago-Jacinto, L. Rendon-Vazquez, J. Nemeth, I. Dekany, D. Diaz, Novel synthesis pathway of ZnO nanoparticles from the spontaneous hydrolysis of zinc carboxylate salts, J. Phys. Chem. B 107 (2003) 12597–12604.
[21] L. Spanhel, M.A. Anderson, Semiconductor clusters in the sol–gel process—quantized aggregation, gelation, and crystal-growth in concentrated ZnO colloids, J. Am. Chem. Soc. 113 (1991) 2826–2833.
[22] M.S. Tokumoto, V. Briois, C.V. Santilli, S.H. Pulcinelli, Preparation of ZnO nanoparticles: structural study of the molecular precursor, J. Sol–Gel Sci. Technol. 26 (2003) 547–551.
[23] B. Baruwati, D.K. Kumar, S.V. Manorama, Hydrothermal synthesis of highly crystalline ZnO nanoparticles: a competitive sensor for LPG and EtOH, Sens. Actuators B 119 (2006) 676–682.
[24] S.C. Zhang, X.G. Li, Preparation of ZnO particles by precipitation transformation method and its inherent formation mechanisms, Colloids Surf. A 226 (2003) 35–44.
[25] L.P. Bauermann, J. Bill, F. Aldinger, Bio-friendly synthesis of ZnO nanoparticles in aqueous solution at near-neutral pH and low temperature, J. Phys. Chem. B 110 (2006) 5182–5185.
[26] K. Fujita, K. Murata, T. Nakazawa, I. Kayama, Crystal shapes of zinc oxide prepared by the homogeneous precipitation method, J. Ceram. Soc. Jpn 92 (1984) 227–230.
[27] A.S. Shaporev, H. Zeng, V.K. Ivanov, Yu.D. Tret'yakov, Mechanism of formation of finely dispersed zinc oxide in homogeneous hydrolysis of zinc nitrate in the presence of hexamethylenetetramine, Dokl. Chem. 426 (2009) 101–104.
[28] B.G. Song, S.N. Cha, J.E. Jung, J.E. Jang, Method for preparing zinc oxide nanostructures and zinc oxide nanostructures prepared by the same, US Patent Application, 20090098043 (2009).
[29] P.Y. Wu, J. Pike, F. Zhang, S.W. Chan, Low-temperature synthesis of zinc oxide nanoparticles, Int. J. Appl. Ceram. Technol. 3 (2006) 272–278.
[30] N. Blazevic, D. Kolbah, B. Belin, V. Sunjic, F. Kajfez, Hexamethylenetetramine, a versatile reagent in organic synthesis, Synthesis 3 (1979) 161–176.
[31] A Aimable, M.T. Buscaglia, V. Buscaglia, P. Bowen, Polymer-assisted precipitation of ZnO nanoparticles with narrow particle size distribution, J. Europ. Ceram. Soc. 30 (2010) 591–598.
[32] M.N.R. Ashfold, R.P. Doherty, N.G. Ndifor-Angwafor, D.J. Riley, Y. Sun, The kinetics of the hydrothermal growth of ZnO nanostructures, Thin Solid Films 515 (2007) 8679–8683.
[33] A. Goldenblum, A.B. Marian, V. Teodorescu, Optical properties of ZnO nanocrystallites embedded in a gold-oxide matrix, J. Optoelectron. Adv. Mater. 8 (2006) 2129–2132.